Polymer 50 (2009) 2706–2715

Contents lists available at ScienceDirect

Polymer

journal homepage: www.elsevier.com/locate/polymer

Critical stress for drawing-induced α crystal–mesophase transition in isotactic polypropylene

Zhe Ma [a,b], Chunguang Shao [a], Xiao Wang [a], Baijin Zhao [a], Xiangyang Li [a], Haining An [a,b], Tingzi Yan [a], Zhongming Li [b], Liangbin Li [a,*]

[a] National Synchrotron Radiation Lab and Department of Polymer Science and Engineering, University of Science and Technology of China, Hefei, China
[b] College of Polymer Science and Engineering and State Key Laboratory of Polymer Materials Engineering, Sichuan University, Chengdu, China

ARTICLE INFO

Article history:
Received 18 November 2008
Received in revised form
13 February 2009
Accepted 4 April 2009
Available online 12 April 2009

Keywords:
Drawing-induced crystal–mesophase transition
Critical true stress
Nucleation theory

ABSTRACT

Drawing-induced α crystal–mesophase transition of isotactic polypropylene (iPP) was studied with in situ wide angle X-ray diffraction (WAXD) during the true stress–true strain tensile testing. The true stress–true strain and in situ WAXD measurements revealed that the critical stress for the crystal–mesophase transition has a nearly linear correlation with lamellar thickness irrespective of the sample processing method, which indicated that superstructures might have minor effect in this aspect. Accordingly, a tentative mechanism of phase transition is proposed based on the ideas of nucleation and dislocation theories. The fitting result shows that the free energy of the stretching-induced mesophase is about 2.5 J/cm^3 lower than that of α crystal at room temperature. The energy barrier for the formation of critical nucleus during the α crystal–mesophase transition is estimated as about 71 k_BT, which is possible to be overcome by the thermal fluctuation. The critical size of the nucleus decreases with the lamellar thickness l_c as well as the critical tensile stress for the crystal–mesophase transition, which is rather similar to the effect of supercooling.

1. Introduction

Phase transition induced by external fields such as shear and stretching is a general phenomenon in polymer materials [1–13], which may occur during processing, mechanical testing and using of polymer products. These external fields provide activation energy to polymer chains to overcome the energy barrier for the initiation of the phase transitions, which may, to some extent, be equivalent to temperature or pressure. Thus for each phase transition a critical stress is expected, which may be related to the state of initial phase, such as size and superstructure in large length scale of this phase. For example, crystal–crystal and crystal–mesophase transitions should have a direct correlation with the lamellar thickness, similar to the correlation between the lamellar thickness and the melting temperature through Thomason–Gibbs equation [14]. Nevertheless, the semicrystalline polymers were composed of hierarchic structures with different length scales, which may also make their contributions on the actually measured stress. Moreover other structural changes are also accompanying with the phase transition, for instance slip, orientations of both the amorphous phase and crystalline phase, and disentanglement of chains. Thus, special designs on the tested samples and experiments are required to obtain such a correlation.

Isotactic polypropylene (iPP) is one of the most important members in polyolefin family and it is a nice model system to study the crystal–mesophase transition. Besides the three crystalline phases, α, β and γ, iPP can also form a mesophase through fast quenching [15–25] or stretching deformation of the α crystal [1–3], which has been widely studied with different focuses during last 60 years. In terms of deformation-induced structure, the emphases of the reported work can be summarized into two groups. One focuses more on the structure information during drawing [1–3,11,26–34]. For example, Hsiao and coauthors [1–3] studied the entanglement and tie chain on the drawing-induced phase transition and the structure of the final mesophase. They found that at room temperature the chain entanglement in amorphous phase acted as the role of transporting the force to fracture the crystal during stretching, whereas at high temperature the chain entanglement disentangled to relax the strain of the tie chain and induce the formation of more folded-chain lamellae. Nozue et al. [27] studied the structure evolution of the parent and the daughter lamellae during drawing. At first the long period of parent lamellae increased and the crystal packing began to disorder along the

* Corresponding author. Tel.: +86 551 3602081; fax: +86 551 5141078.
E-mail address: lbli@ustc.edu.cn (L. Li).

0032-3861/$ – see front matter © 2009 Elsevier Ltd. All rights reserved.
doi:10.1016/j.polymer.2009.04.010

a-axis, while the long periods of parent and daughter lamellae drastically started to decrease accompanying with necking. A linear correlation between the orientations of crystalline and amorphous phases was established by Song et al., which had a slope of 1.85 during the necking process [28,29]. A serial elegant work from De Rosa et al. correlated mechanical properties with stereoregularity and the structure–mechanical phase diagrams of iPP and syndiotactic polypropylene (sPP) were reported [11–13]. Besides the α crystal of iPP, the stretching behaviors of β crystal were also investigated widely [30–34]. Drawing-induced phase transitions has been observed on many other polymers such as poly(ethylene terephthalate) (PET) [4–8], poly(lactic acid) (PLA) [9], poly-(vinylidene fluoride) (PVDF) [10] and etc.

The other group [35–51] places more emphasis on the mechanical properties. With a video-controlled testing system, G'Sell et al. measured the true stress–true strain curves of many polymers [39–41]. Meijer and coauthors [42–48] have done systemic works to investigate the relation between macroscopic deformation behavior (yield stress, strain softening and strain hardening) and the intrinsic molecular characteristics (crystallinity, lamellar thickness and entanglement density) of polymers including both the amorphous polymers and the semicrystalline polymers. Men et al. [49] mainly focused on the effect of the entangled amorphous network on the drawing for the semicrystalline polymers. They found that the critical strain at onset of the crystalline block disaggregation–recrystallization was decided by the interplay between the state of the amorphous phase and the intrinsic stability of crystal block, in which the tie molecules was not the decisive factor in determining the stretching strength. Associating with the qualitative structural changes of the deformation mechanism, Strobl and coauthors [50,51] have marked four points in the stress–strain curve in relation to (A) the onset of the isolated inter- and intralamellar slip process, (B) a change into a collective activity of slips, (C) the beginning of crystallite fragmentation and (D) chain disentanglement. The corresponding critical properties are decided by the intrinsic structures such as lamellar thickness and superstructures, which have been studied by some authors.

How much energy is required from the stretching to help molecular chains to overcome the energy barrier of the α crystal–mesophase transition? To answer this question requires a close combination of structure measurements and mechanical testing. In this work, iPP is taken as the model system to study the critical stress required for the α crystal–mesophase transition. Two groups of samples were designed for this target. Similar to the study on the correlation between melting temperature and lamellar thickness, structures were designed to form at constant temperature rather than non-isothermal process. The first group of samples were first quenched to liquid N_2 and subsequently annealed at different elevated temperatures to obtain different lamellar thickness. This approach could vary the superstructures different from that formed by isothermally crystallization. The second group of samples was prepared through direct crystallization at the same temperatures for annealing the samples of the first group. This approach allows us to check whether superstructure influences the critical stress for crystal–mesophase transition. It is also noted that the common engineering stress is not valid for the current mechanism study. Thus in our tensile experiments, both the true stress and true strain were measured, which were the actual external fields that the polymer felt. Combining the true stress–true strain and in situ wide angle X-ray diffraction (WAXD) measurements, the critical stresses of the crystal–mesophase transition for lamella with different thickness were obtained, which showed a linear correlation. This allows us to interpret the stress-induced phase transition based on nucleation theory and calculate the energy barrier for critical nucleus for the drawing-induced crystal–mesophase transition.

2. Experimental

The high molecular mass isotactic polypropylene was supplied by SABIC-Europe, which has a melt flow index of about 0.3 g/10 min (230 °C/2.16 kg, ASTM D1238) and an average molecular weight M_n and M_w of about 150 and 720 kg/mol, respectively. The tacticity and melting point are about 98% and 165 °C, respectively. The iPP granules were pressed into thin plates with a thickness of about 1 mm at 220 °C first. The iPP thin plates covered by aluminum foil were heated and held at 220 °C for 5 min to erase the memory effect. (i) For the first group, samples were quenched to liquid N_2 and then put into the oven at 40, 80, 120 and 140 °C to anneal; note that as the thickness of the samples is 1 mm, the initially quenched samples contain mesophase and α crystals, which transformed into fully α crystals after annealing, as supported by WAXD measurement. (ii) For the second group, samples were quickly moved into isothermal water at 80 °C or oven at 120 and 140 °C. When the iPP was quenched to 80 °C, the estimated cooling rate was up to 10,000 °C/min. Additionally, 80 °C was not low enough to form mesophase and higher than the homogeneous nucleation temperature, where the sample still had the feature of the crystallized iPP with the superstructure of spherulite, so in order to discuss the influence of the lamellar aggregation, the iPP quenched to and isothermally processed at 80 °C could also be classified to be one of the crystallized samples. The experiments in oven were under the protection of nitrogen gas. To avoid the possible effect of different crystallinities on the critical behavior, all samples were annealed or crystallized for 8 h to make the crystallinities as close as possible. The annealed and isothermally crystallized iPP films were cut into dumbbell-shape with a total length and a neck width of 29 mm and 4 mm, respectively. Subsequently, the samples were placed in the experimental environment for 24 h for the conditioning.

Tensile experiments were carried out under the controlled experimental room temperature (25 °C). Samples were mounted between two clamps of the home-made miniature mechanical test apparatus. The drawing-speed was chosen to be 1.16 μm/s. Error of the force sensor was around 1 N. A charge coupled device (CCD) camera with the recording frequency of one frame per 10 s was equipped in the testing apparatus to record the change of the size during drawing in order to calculate the true stress and the true strain. The CCD camera recorded the change of both the width and the thickness during drawing and the various value of the cross-section area can be calculated supposing the deformation is affine. Hence, the true stress can be calculated through dividing the tensile force*F* by the corresponding cross-section area *A*, namely $\sigma = F/A$. The true strain is defined as $\varepsilon = \Delta L/L$. Assuming the volume keeps constant in the drawing process, the true stain can be calculated with the following equation $\varepsilon = A_0/A - 1$, where A_0 denotes the initial cross-section area.

During the drawing, the in situ WAXD measurements were performed on the setup with Mar 300 image plate as the detector and Mo Kα as the X-ray source (wavelength $\lambda = 0.07107$ nm). The sample-to-detector distance was 226 mm.

The one-dimensional WAXD curves were fitted according to Gaussian functions to obtain the crystallinities of the initial samples. The degree of orientation of the crystal was generally expressed by the orientation parameter defined by

$$S_{hkl} = \frac{3\langle \cos^2 \phi_{hkl} \rangle - 1}{2}, \quad (1)$$

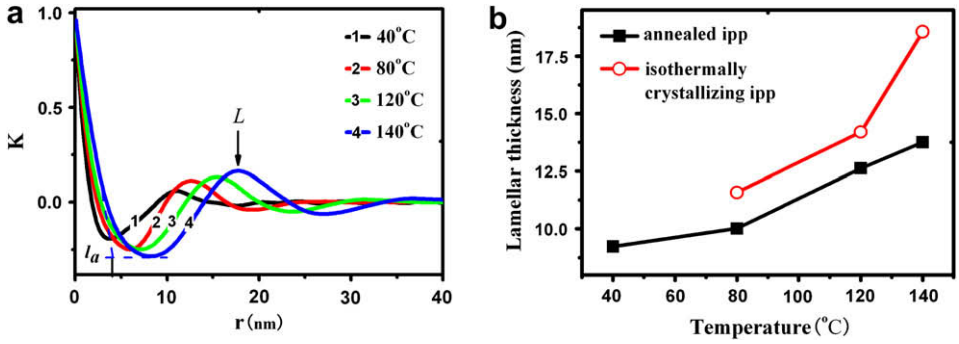

Fig. 1. (a) The one-dimensional correlation function $K(r)$ for lamellae annealed at different temperatures; (b) the lamellar thickness of annealed (solid square) and isothermally crystallized iPP samples (open circle) formed at different temperatures.

where the angle ϕ denotes the angle between the axis of interest and the unique axis. The drawing direction is chosen as the reference axis to calculate the orientation by the normal vector of the lattice plane (hkl). Hence, $\langle\cos^2\phi_{hkl}\rangle$ can be got from azimuthal scattering intensity distribution by the following equation

$$\left\langle \cos^2\phi_{hkl} \right\rangle = \frac{\int_0^{\pi/2} I_{hkl}(\phi)\cos^2\phi\sin\phi d_\phi}{\int_0^{\pi/2} I_{hkl}(\phi)\sin\phi d_\phi}, \quad (2)$$

where $I_{hkl}(\phi)$ is the scattering intensity along the angle ϕ. The orientation parameter attains a value of unity when all the crystals are oriented with their interested axis parallel to the reference direction (i.e., the stretching direction), a value of -0.5 corresponds to a state that all the interested axes are perpendicular to the reference direction, while totally random orientation gives a value of 0. For our purpose, the orientation parameter was calculated through the Picken's method from the (110) reflection of WAXD for iPP [52]. During the drawing, the beginning of crystal–mesophase transformation was determined by the onset point of the 2θ up-rising of the first peak, which is a combination of (110) reflection of α crystal and the first scattering peak of mesophase.

The SAXS measurements were carried on the synchrotron light source (wavelength $\lambda = 0.154$ nm) with the MarCCD as the detector at National Synchrotron Radiation Laboratory, China. The SAXS covered a range of scattering vector q from 0.14 to 1.4 nm^{-1}. The sample-to-detector distance calibrated by using silver behenate was 992 mm.

The Fit2D software package was used to analyze the two-dimensional (2D) SAXS and WAXD patterns. The SAXS data were analyzed using the one-dimensional correlation function, which is expressed as:

$$K(r) = \left[\int_0^\infty Iq^2\cos(qr)\mathrm{d}q\right]/Q, \quad (3)$$

where Q is the so-called invariant and defined as $Q = \int_0^\infty Iq^2\mathrm{d}q$. From one dimension correlation function $K(r)$ shown in Fig. 1a, the long period L can be determined from the position of the first maximum and the thickness of one phase can obtained from the baseline of the first minimum [53]. Because the thickness directly obtained from the correlation function is the minor part, it was defined as that of amorphous phase l_a. Therefore the lamellar spacing $l_c = L - l_a$.

3. Results

Fig. 1a shows the correlation function for the lamellar stacks formed through annealing at different temperatures. Upon increasing the annealing temperature, the first peaks of the curves shift to large r value, indicating an increase of long period. Based on the correlation function, lamellar thicknesses of all iPP samples are obtained (Fig. 1b). Sample annealed or crystallized at higher temperature has a larger lamellar thickness. The lamellar thicknesses of annealed samples vary from 9.2 to 13.7 nm, while those of the isothermally crystallized iPP range from 11.6 to 18.6 nm. At the same temperature, the isothermally crystallized lamellae are always thicker than those formed through annealing. Using different methods, the desirable samples with various lamellar thicknesses are obtained.

The crystallinities of iPP formed by annealing at different temperatures are compared in Fig. 2a. The crystallinity of iPP annealed at 40 °C is the lowest, while the crystallinity increases a little among the applied temperatures in a range from 47% to 55%. The crystallinities of the isothermally crystallized samples are nearly constant at different temperatures, which changes from 50% to 53% (see Fig. 2b). The close crystallinities can minimize the possible additional effect of crystallinity.

By WAXD, it can be concluded that monoclinic lamellae were present, based on which SAXS showed the formation of lamellar stacks in all samples. The peak width of SAXS indicates that at the same temperature the correlation length of lamellar stack increases with the increase of temperature, which, however, does not show an obvious difference between annealed and crystallized samples. To specify the superstructure difference in a large length scale, all samples were cut by microtome and the superstructure morphologies were studied using polarized light optical microscope (PLOM). As shown in the PLOM micrographs of samples annealed and isothermally crystallized at 120 °C (Fig. 3), a great difference exists between the two groups of samples. The morphology of large spherulite could be clearly seen in the isothermally crystallized samples, while no clear spherulitic feature was distinguished on the annealed samples. If there is, the size should be too small to be observed with polarized light optical microscope. Additionally, we also did the step heating experiment with the increment of 10 °C to enhance the contrast so as to observe the sample formed by annealing at 140 °C. During the whole heating process up to melting, no obvious spherulitic feature was distinguished in the polarized light optical microscopy, confirming the difference in the superstructure between the annealed samples and isothermally crystallized samples.

The structure evolution of the annealed or crystallized iPP samples was monitored with in situ WAXD during the drawing

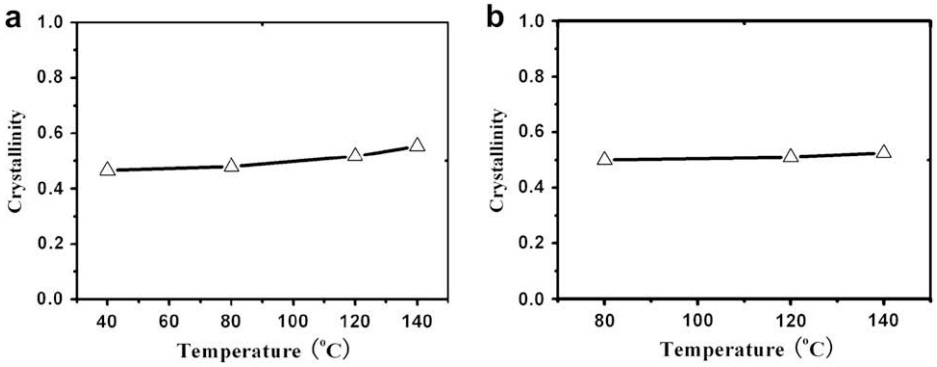

Fig. 2. Crystallinities of (a) annealed and (b) isothermally crystallized iPP samples formed at different temperatures.

where the true stress and true strain were recorded. A representative true stress–true strain curve of iPP is plotted in Fig. 4a, which was initially annealed at 140 °C for 8 h. The true stress quickly reaches the yield point and sharply drops to 27.4 MPa, which is followed by a continuous increase of the true stress due to strain hardening. Five representative two-dimensional (2D) WAXD patterns during stretching are inserted in Fig. 4a with the number indicating their corresponding position in the true stress–true strain curve. The azimuthal intensity curves during stretching are presented in Fig. 4b. The azimuthal angle scans from the stretching direction, which is the vertical direction in the 2D WAXD images in Fig. 4. For clarification we only give some selected curves and mark the onset of lamellar orientation. The orientation parameters are calculated from Fig. 4b and plotted in Fig. 4c to show how the change happens during drawing. In Fig. 4c the initial orientation parameter of 0.15 from the isotropic sample is mainly due to the shadow of the clamps, with minor additional effect of sample absorption, since the samples are dumbbell-shape and the clamps are just in the light path of the air scattering giving a shadow in the length (stretching) direction. By WAXD one can find the onset point for orientation in Fig. 4c, then by using the simultaneous tensile testing, the corresponding critical mechanical properties were determined according to the stress and strain curve in Fig. 4a. The crystal begins to orient at the critical point with a true strain and a true stress of 0.49 and 39.16 MPa respectively. In this process, the crystal transition also occurs from α form to mesophase, which can show both characteristic peaks shifting to the values of mesophase in one-dimensional (1D) WAXD curve at the beginning of phase transition and its fingerprint of the typical six reflection points in 2D WAXD pattern at the end of stretching experiments. The change of (040) and (130) peaks in the 2D patterns seemed very large in the meridional direction, but the disappearance and combination of these two distinguished peaks and the appearance of a wider peak occurred simultaneously. It is difficult to precisely judge the starting point of the phase transition by the change of these two peaks. Additionally, the error bar for crystallinity fitting during stretching is relatively large for judging the phase start. Therefore, the position of first peak in 1D WAXD curves is chosen to judge when the crystal transition starts, as shown in Fig. 4d and e. This method introduces less artifact of data analysis. For the convenience of description, the onset of phase transition is defined as the "critical" point, and the critical mechanical properties could be gotten in the same way as described above for the orientation. For iPP annealed at 140 °C, the critical strain and stress for the crystal–mesophase transition are 0.49 and 39.2 MPa, respectively, which are the same as those for the onset of orientation.

All the true stress–true strain curves of iPP annealed at different temperatures are summarized in Fig. 5, in which the crystal–mesophase transition points are marked. A drop of true stress is observed after the yielding, which is similar with that in the compression experiment done by Meijer et al. [47], but different from the report of G'Sell et al. [40] on tensile testing. Although the discussion about strain softening is outside the scope of this article, it should be noted that in the experiment of G'Sell, the samples prepared through directly machining extruded rod should still keep the oriented structure, which is very evident in the extruding process, while melting process experienced by our samples might erase the orientation of structure. Also, Meijer et al. [48] have pointed that the orientation would markedly influence the tensile property for drawing experiments. Hence, it is speculated that the drop of the true stress in our results was caused by the thermal processing of sample preparation.

The critical stresses for the stretching-induced lamellar orientation and the crystal–mesophase transition of iPP samples are plotted vs the annealing temperature in Fig. 6. The critical stresses for the stretching-induced orientation increase from 22.1 to

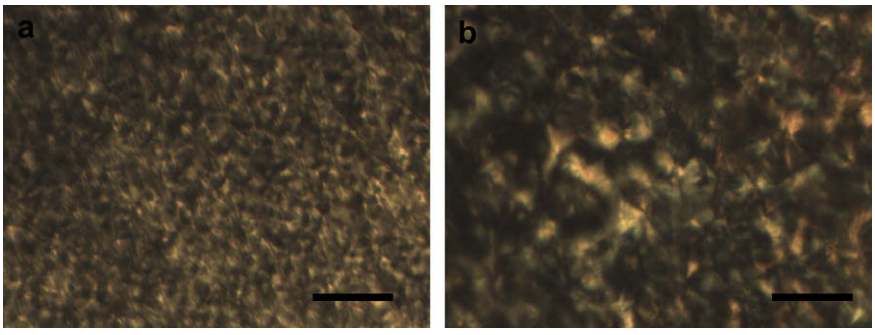

Fig. 3. PLOM micrographs of samples (a) annealed and (b) isothermally crystallized at 120 °C. The scale bar represents 100 μm.

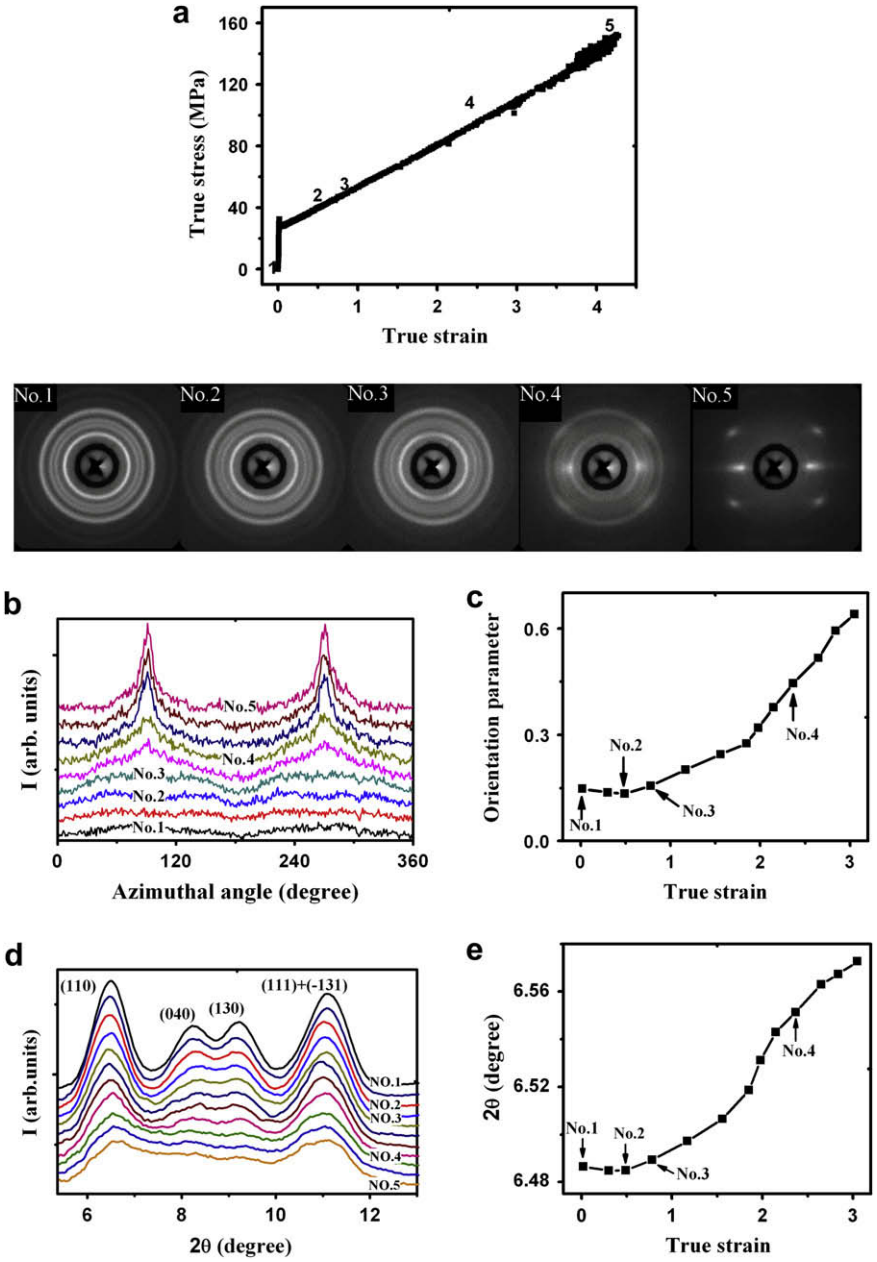

Fig. 4. (a) True stress–true strain curve and selected WAXD 2D images at different strains, (b) azimuthal intensity curves, (c) orientation parameters, (d) one-dimensional WAXD intensity curves, (e) 2θ value of the first peak in the one-dimensional WAXD curves of iPP sample annealed at 140 °C.

39.2 MPa for iPP annealed at 40, 80, 120, 140 °C, respectively, which increase with temperatures. Similarly, the critical stresses for the crystal–mesophase transition also increase with the annealing temperature, indicating that a higher energy for samples annealed at higher temperature is required to promote the crystal–mesophase transition. Comparing the critical stresses for the crystal–mesophase transition and the lamellar orientation, two processes occur at the same stress for all annealed samples except the one annealed at 120 °C, whose orientation takes place slightly earlier than the crystal–mesophase transition. Note that the orientation is generally accompanied with fibrillation, which is in a scale up to micrometer, whereas crystal–mesophase transition relates with molecular packing in a length scale of sub-nanometer. Due to the interconnectivity, it is hard to completely decouple the structural changes in different scales during the whole drawing

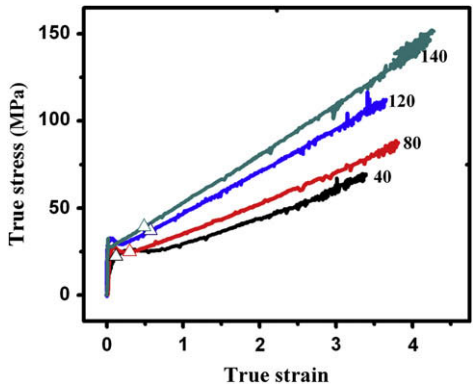

Fig. 5. True stress–true strain curves of iPP samples annealed at different temperatures.

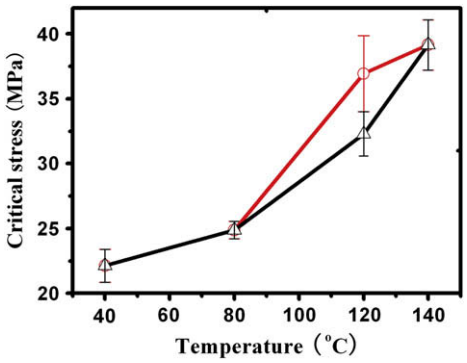

Fig. 6. True stresses at the onset of orientation (black triangle) and the crystal–mesophase transition (red circle) of iPP samples annealed at different temperatures. (For interpretation of the references to color in this figure legend, the reader is referred to the web version of this article.)

process, where the structural changes may occur simultaneously or in sequence.

The WAXD curves on the final states of the annealed iPP samples after stretching are summarized in Fig. 7. The first peak locates between the diffraction peaks of the mesophase obtained by fast quenching and α form crystal, which indicates the stretching-induced mesophase may be different from the quenched one. Minor α phase may also survive at the end of stretching.

The same WAXD and the true stress–true strain measurements were also carried on iPP samples that were isothermally crystallized at the same temperatures as used for annealing. The true stress–true strain curves are presented in Fig. 8. The critical stresses for the beginning of orientation and the crystal–mesophase transition were plotted vs the crystallization temperatures in Fig. 9, which are different from those of annealed iPP samples. The critical stresses for the onset of orientation and the crystal–mesophase transition follow the same trend, which always increase with the temperatures. For the convenience of comparison the structural and mechanical data of all samples are summarized in Table 1.

The final 1D WAXD curves after drawing are shown in Fig. 10. Samples crystallized at high temperatures give clear reflection peaks of α crystal, indicating the surviving of some α crystals.

4. Discussion

In this section, we would like to focus on the relation between structural information and the critical point. When studying the critical stress for yield point, most previous studies by others present the yield stress related to the lamellar thickness, which can be explained by the screw dislocation model first proposed by Yang

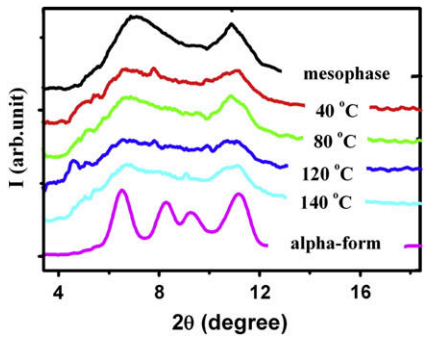

Fig. 7. The one-dimensional WAXD curves of iPP samples annealed at different temperatures after stretching.

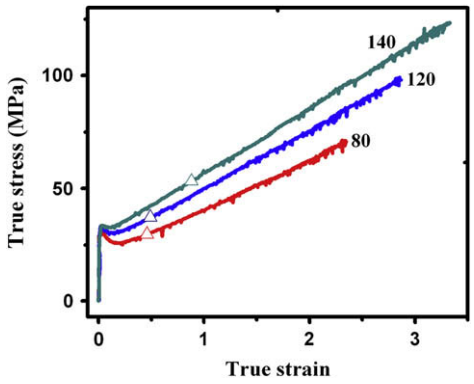

Fig. 8. True stress–true strain curves of iPP samples isothermally crystallized at different temperatures.

[54] and developed by Shadrake and Guiu [55]. Although this model, to some extent, begins to quantitatively explain the relation between the stress and lamellar thickness, its physical meaning is not verified yet, because no one has surely proven that the screw dislocation happens at the yield point of polymer. However, for phase transition from α crystal to mesophase, the characteristic structural changes in the chain arrangement can be directly detected from order to disorder with WAXD. Thus, in this section, we will mainly discuss with the relation between the critical stress for the crystal–mesophase transition, namely the lamellar lattice disordering, and its intrinsic structure, the lamellar thickness, when the crystallinities are close. Additionally, the relation between drawing-induced lamellar orientation and the crystal–mesophase transition is discussed.

The critical stresses for phase transition are 22.1, 24.9, 36.9, 39.2 MPa for iPP samples annealed at 40, 80, 120, 140 °C, while those of the isothermally crystallized iPP samples range from 29.6 to 53.2 MPa. All experimental results show that samples annealed or crystallized at higher temperature can sustain larger stress before the onset of the lamellar orientation and the crystal–mesophase transition. Combining the lamellar thickness from Fig. 1b and the critical stresses from Figs. 5 and 8, we plot the critical stress for the crystal–mesophase transition vs lamellar thickness of all samples in Fig. 11. The stress error is mainly caused by the time resolution of WAXD measurements. It seems that all points fall in one straight line within experimental error. This suggests that crystallization and annealing do not make obvious difference in this aspect. In other words, lamellar thickness seems to be the dominant factor controlling the critical stress for the crystal–mesophase

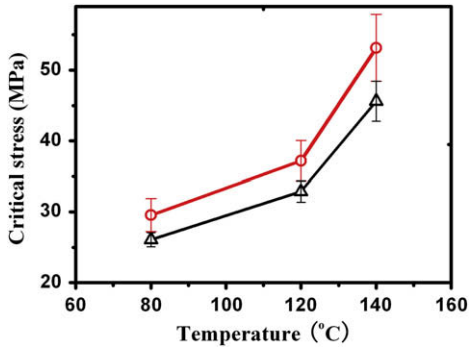

Fig. 9. True stresses at the onset of orientation (black triangle) and the crystal–mesophase transition (red circle) of iPP samples isothermally crystallized at different temperatures. (For interpretation of the references to color in this figure legend, the reader is referred to the web version of this article.)

Table 1
The structural and mechanical data of all samples processed at different temperatures.

	Temperature (°C)	Crystallinity	l_c (nm)	Orientation		Crystal transition	
				Critical strain	Critical stress (MPa)	Critical strain	Critical stress (MPa)
Annealed samples	40	0.47	9.2	0.12	22.1	0.12	22.1
	80	0.48	10.0	0.30	24.9	0.30	24.9
	120	0.52	12.6	0.36	32.3	0.57	36.9
	140	0.55	13.7	0.49	39.2	0.49	39.2
Crystallized samples	80	0.50	11.6	0.24	26.1	0.46	29.6
	120	0.51	14.2	0.31	32.9	0.49	37.2
	140	0.53	18.6	0.60	45.6	0.88	53.2

transition, while superstructure such as spherulite may have minor effect on this point.

To explain lamellar thickness dependence of the critical stress, a model of phase transition was presented and schematically shown in Fig. 12. According to the nucleation theory already applied in the crystallization from melt, the phase transition in solid should start with the nucleation of mesophase from the initial α crystal phase. The mesophase nucleus is generated through moving adjacent chains up and down in c axis direction with a displacement of d by the stress. As shown in Fig. 12, r^* is the radius of the critical nucleus, l_c is the lamellar thickness and τ is the applied shear stress. The change of the Gibbs free energy ΔG related to the formation of the mesophase nucleus with a radius of r can be formulated as following:

$$\Delta G = \Delta G_f + \sum A\gamma - W. \quad (4)$$

In right side of Eq. (4), the first term ΔG_f is the difference between the bulk free energy of the final mesophase and the original α crystal. The second term is the total surface free energy, which is brought by the interface between the initial α crystal and the nucleus of the mesophase. A and γ are, respectively, the surface area and the corresponding specific surface free energy. Actually the total surface free energy should include those of both the side and end surfaces, but in our model the end surfaces already exist for the initial α phase. Thus for simplification, the change of the end surface energy can be neglected and the third term is the contribution of the work done by the external force, which does not exist in the quiescent condition. The introduction of the external work breaks the thermodynamic equilibrium and makes the impossible transition at static state happen.

Hence, the Gibbs free energy ΔG associated with nucleation of the mesophase with a lamellar thickness of l_c and a moving distance of $c/3$ in the chain direction under a shear stress of τ can be expressed as the following:

$$\Delta G = \pi r^2 l_c \Delta g_f + 2\pi r l_c \gamma_l - \frac{n}{2} \times \pi a l_c \tau \times \frac{c}{3}. \quad (5)$$

Here, Δg_f is the difference of bulk free energies per unit volume between α crystal and mesophase, γ_l is the specific surface free energy of the lateral surface and a is the diameter of the helix which approximately equals the lattice constant a of α phase. The nucleus was set to have the same thickness as that of the lamella, which is justified by the following reason. If the size of the nucleus in the chain direction is smaller than the lamellar thickness, a deformation region or defect would exist inside lamella, which will suffer a larger elastic penalty than the energy required to shifting $c/3$ of the whole crystalline segment l_c. In other words, even if the elastic deformation region is generated inside lamella, it will easily diffuse from the inner to the surface. Thus, a nucleus with the same thickness as l_c requires the lowest energy barrier. n is the number of chains included in the critical nucleus $n = 4\pi r^2/ab$, where a and b are the lattice constants of α phase and each unit cell contains 4 chains. It is assumed that half of the chains will move up and down, respectively, in a relative displacement of $c/3$. Assuming the displacement of $c/3$ is due to the 3/1 helix in the α crystal and mesophase and c/3 is large enough for the deformation to induce the system unstable. The lamellar thickness l_c should be replaced by the stem length [56]. Whereas for iPP, the angle between the chain axis and the fold surface is 99.3°, thus the stem length approximately equals the lamellar thickness. The radius r^* of the critical mesophase nucleus can be obtained through the deviation of ΔG ($d\Delta G/dr = 0$), resulting in:

$$r^* = \frac{3b\gamma_l}{2\pi c\tau - 3b\Delta g_f}. \quad (6)$$

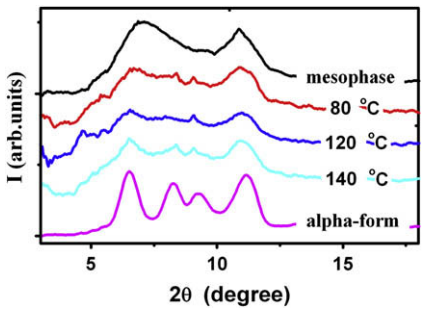

Fig. 10. The one-dimensional WAXD curves of iPP samples isothermally crystallized at different temperatures after stretching.

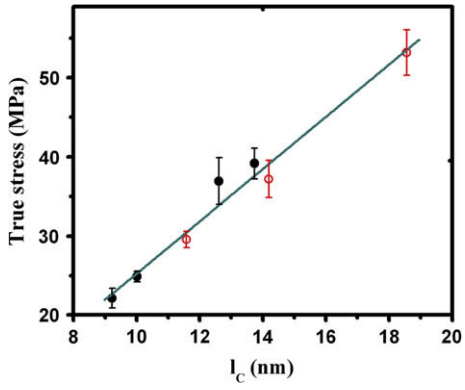

Fig. 11. The critical stresses for the crystal–mesophase transition of the annealed (black solid) and the crystallized (red open) iPP samples with different lamellar thicknesses. (For interpretation of the references to color in this figure legend, the reader is referred to the web version of this article.)

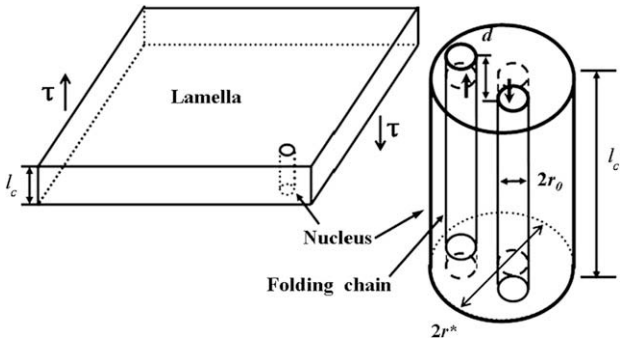

Fig. 12. Schematic illustration of the nucleus of the mesophase in a lamella.

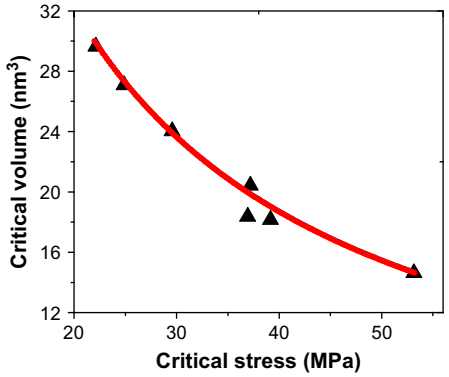

Fig. 13. The plot of the critical volume of nucleus vs the critical stress for the crystal–mesophase transition.

To form a nucleus with a critical size r^* requires overcoming an energy barrier ΔG^*, which can be formulated as:

$$\Delta G^* = \frac{3\pi b l_c \gamma_l^2}{2\pi c\tau - 3b\Delta g_f}. \quad (7)$$

As in the dislocation theory on yield, the Tresca yield criterion, $\sigma = 2\tau$, is assumed to be valid for the critical phase transition stress, as a sliding of chains is required in both cases [38,54–56]. Then, the relationship between the critical stress for phase transition and the lamellar thickness l_c can be written as:

$$\sigma = 2\tau = \frac{3b\gamma_l^2}{c\Delta G^*} l_c + \frac{3b\Delta g_f}{\pi c}. \quad (8)$$

In order to obtain ΔG^* and Δg_f, the critical tensile stress vs the lamellar thickness is plotted in Fig. 11, which presents a good linear relationship. From the intercept and the slope of the linear fitting, the $\gamma_l/\Delta G^*$ and Δg_f can be obtained. The bulk free energy difference Δg_f is -2.5 J/cm^3. The negative value of Δg_f is rather unexpected, as the thermally formed mesophase is generally recognized as metastable, compared to α crystal. The negative Δg_f suggests that the stretching-induced mesophase is more stable than α crystal at room temperature. It should be emphasized that there are some differences between the thermally formed and the drawing-induced mesophases. First, Ran et al. [1] found that the drawing-induced mesophase in iPP fiber had no obvious long period, which did exist in the thermally formed mesophase. Second, the drawing-induced mesophase should be oriented, while the thermally formed mesophase must be isotropic. Qiu et al. [26] found the stretched mesophase was more stable than the original quench-induced mesophase. Though we cannot distinguish the obvious difference between these two mesophases by WAXD, DSC indeed tells us the different stability. Based on Thomas–Gibbs equation, we speculate the size may be the key. As thermally formed mesophase has a dimension of about 4 nm, while drawing-induced mesophase does not have a long period which can be long fibrillar domains. This will dramatically change the thermal stability, similar to the difference between extended-chain and folded-chain crystals.

Because Δg_f is contributed from both enthalpy and entropy and the bulk free energy difference can be expressed as $\Delta g_f = \Delta h - T\Delta s$, a negative Δg_f may be true for two reasons. First, based on WAXD and DSC data, the enthalpy difference per unit weight of mesophase and α crystal was estimated. Dividing the value of melting enthalpy of stretched mesophase by its crystallinity, the melting enthalpy per unit weight of 100% mesophase is determined as 145 J/g, which was very close to 150 J/g, the value of the 100% α crystal calculated in the same way. Additionally considering their different densities, it can be reliably concluded that the difference in melting enthalpy per unit volume between the stretched mesophase and α crystal is very small. Thus, the enthalpy was the minor factor in deciding the phase transition. Second, it is well known that the entropy of the mesophase is much higher than that of α crystal because of the randomness of the packing and the hands of helices. The high entropy of the mesophase helps to stabilize the system. Combining the small difference of enthalpy and the favorable entropy, the drawing-induced mesophase is more stable than the α crystal can be justified.

Is the energy barrier low enough for the thermal fluctuation to overcome under the external force? Assuming the lateral surface energy γ_l is 10 erg/cm^2 [57], the calculated indicator of the energy barrier ΔG^* is 2.9×10^{-19} J (71 k_BT, where k_B is the Boltzmann constant). Similar to that applied in the dislocation theory, this value is in the range of 40–80 k_BT for thermal fluctuation to induce dislocation through chain sliding. Thus, the external force reduces the nucleation barrier for the crystal–mesophase transition and makes the nucleation possible through thermal fluctuation.

Inserting the above calculated value of Δg_f into Eq. (6), the critical nucleus sizes of mesophase can be obtained, which are plotted vs the critical stress for the crystal–mesophase transition in Fig. 13. We use the volume of the critical nucleus instead of radius r^* to take into account the difference of l_c. A larger critical stress corresponds to a smaller volume of critical nucleus. With the increase of the thickness l_c, the lamellae will become more difficult to deform, which requires a larger stress according to Eq. (8). Correspondingly, the larger stress contributes more to reduce the energy barrier and a smaller critical nucleus size is required to kick off the phase transition. This mechanism is rather similar to the effect of supercooling. Nucleation under larger stress is equivalent as that under larger supercooling, which has a smaller energy barrier to overcome and a smaller critical nucleus is required.

We would like to point out that the model developed in this work is for the stress-induced phase transition rather than yielding, though both are assumed to have a nucleation process and we borrowed some idea from dislocation theory. For yielding process nucleation is to generate the dislocations, while for crystal–mesophase transition nucleation is to initiate the growth of the new phase. Thus the consequences of two processes are completely different. Yielding cuts large crystal into small crystals, while the crystal–mesophase transition leads to the formation of the new phase, which is not necessarily with smaller size than that of the parent phase. As the same with the temperature limit of dislocation applied on the behavior of yielding [54,56], the nucleation model for the crystal–mesophase transition should also have the applied temperature range. At high temperatures the stretching may not induce the crystal–mesophase transition [1,3], instead it

may induce a liquid or amorphous–crystal transition. Nevertheless the generic idea of the stress-induced phase transition should also hold at high temperatures, where the external work is to overcome the elastic retraction and promote the orientation and stretch of chains.

In addition to the crystal–mesophase transition, other structural change also occurs during stretching. Comparing the critical stresses (or strains) for crystal–mesophase transition and the onset of lamellar orientation (Figs. 6 and 9), the drawing-induced orientation occurs slightly earlier than the crystal–mesophase transition does for samples isothermally crystallized at 80, 120 and 140 °C and sample annealed at 120 °C, while the orientation and the crystal–mesophase transition take place at the same time for all annealed samples except at 120 °C. No sample shows that crystal–mesophase transition happens earlier than the orientation does. Distinguishing the occurrences of orientation and phase transition actually is to compare the critical stress, namely studying how structure changes with temperature and how the structure influences the critical stress. The critical stress for α crystal–mesophase transition was decided by the lamellar thickness, while that for orientation might be influenced by both the lamellar and superstructures, at least from our results. There are two possible mechanisms to explain stretch-induced orientation. One is rotation of lamellar stacks, another is the stretch-induced melting and recrystallization. From our result, both cases may occur while the first one should be the dominant one. Irrespective of any other cases, the stretch-induced orientation is determined by the dimension of the lamellar stack and the interaction among them or the coherence strength of the superstructure. Comparing with annealing at the same temperature, crystallization leads to thick crystals and regular lamellar stacks, which increase the intralamellar force and weaken the interaction among lamellar stacks. The former will increase the critical stress for the phase transition and the latter will make the lamellae easier to rotate. This may be the reason that orientation occurs with a smaller stress than the crystal–mesophase transition takes place for the crystallized samples. The orientation and the crystal–mesophase transition happen simultaneously in most of the annealing samples, which certainly is a coupling process. Nevertheless, currently we cannot find a precise reason for the exceptional case at 120 °C, as current detailed structure information among the lamellar stacks is difficult to obtain. Therefore, essentially whether orientation or crystal–mesophase transition occurs first is determined by the values of the coherence energies of lamellar crystals and superstructure.

5. Conclusion

With the different processing methods, two groups of samples with various structures were prepared for studying the crystal–mesophase transition. The quenched iPP samples were annealed to vary the lamellar thickness and change the effects of the superstructure for studying the influence of the lamellar thickness on the stretching-induced structural changes, while the isothermally crystallized iPP samples contain the lamellae with different thicknesses and the different superstructures. The WAXD results revealed the critical stress at the onset of α crystal–mesophase transition increased with the increase of the lamellar thickness, irrespective of the processing methods. A nearly linear relationship between the critical stress and the lamellar thickness for all iPP samples was obtained, which indicates the superstructures do not affect the correlation significantly. We proposed a simple model to account the stretching-induced crystal–mesophase transition in which the transition was considered to start with the nucleation of the mesophase. The work done by the external force reduces the nucleation barrier, allowing thermal fluctuation to overcome. The critical nucleation barrier ΔG^* and bulk free energy difference Δg_f are calculated to be 2.9×10^{-19} J (71 k_BT) and -2.5 J/cm^3, respectively.

Acknowledgements

The authors would like to extend their thanks to Dr. Bing Na for helpful discussion and comments on our manuscript. This work is supported by the National Natural Science Foundation of China (50503015, 20774091) as well as the 'NCET' program of the Minister of Education. The research is also in part supported by the Opening Project of the State Key Laboratory of Polymer Materials Engineering (Sichuan University).

References

[1] Ran S, Zong X, Fang D, Hsiao BS, Chu B, Phillips RA. Macromolecules 2001;34:2569–78.
[2] Ran S, Zong X, Fang D, Hsiao BS, Chu B, Cunniff PM, et al. J Mater Sci 2001;36:3071–7.
[3] Zuo F, Keum JK, Chen X, Hsiao BS, Chen H, Lai SY, et al. Polymer 2007;48:6867–80.
[4] Ran S, Wang Z, Burger C, Chu B, Hsiao BS. Macromolecules 2002;35:10102–7.
[5] Kawakami D, Ran S, Burger C, Fu B, Sics I, Chu B, et al. Macromolecules 2003;36:9275–80.
[6] Kawakami D, Hsiao BJ, Ran S, Burger C, Fu B, Sics I, et al. Polymer 2004;45:905–18.
[7] Kawakami D, Hsiao BS, Burger C, Ran S, Avila-Orta C, Sics I, et al. Macromolecules 2005;38:91–103.
[8] Welsh GE, Blundell DJ, Windle AH. Macromolecules 1998;31:7562–5.
[9] Mulligan J, Cakmak M. Macromolecules 2005;38:2333–44.
[10] Wu J, Schultz JM, Yeh F, Hsiao BS, Chu B. Macromolecules 2000;33:1765–77.
[11] De Rosa C, Auriemma F. J Am Chem Soc 2006;128:11024–5.
[12] De Rosa C, Auriemma F, Ruiz de Ballesteros O. Phys Rev Lett 2006;96:167801/1–4.
[13] Ruiz de Ballesteros O, Auriemma F, De Rosa C. Macromolecules 2007;40:611–22.
[14] Wunderlich B. Macromolecular physics. In: Crystal melting, vol. 3. New York, London: Academic Press; 1973. p. 30.
[15] Natta G, Peraldo M, Corradini P. Rend Accad Naz Lincei 1959;26:14–7.
[16] Natta G, Corradini P. Nuovo Cimento Suppl 1960;15:40–51.
[17] Miller RL. Polymer 1960;1:135–43.
[18] Farrow GJ. Appl Polym Sci 1965;9:1227–32.
[19] Corradini P, Petraccone V, de Rosa C, Guerra G. Macromolecules 1986;19:2699–703.
[20] Wyckoff HW. J Polym Sci 1962;62:83–114.
[21] Gailey JA, Ralston PH. Plast Eng Trans 1964;4:29–33.
[22] Gezovich DM, Geil PH. Polym Eng Sci 1968;8:202–9.
[23] McAllister PB, Carter TJ, Hinde RM. J Polym Sci Polym Phys Ed 1978;16:49–57.
[24] De Candia F, Iannelli P, Staulo G, Vittoria V. Colloid Polym Sci 1988;266:608–13.
[25] Wang Z, Hsiao BS, Srinivas S, Brown GM, Tsou AH, Cheng SZD, et al. Polymer 2001;42:7561–6.
[26] Qiu J, Wang Z, Yang L, Zhao J, Niu Y, Hsiao BS. Polymer 2007;48:6934–47.
[27] Nozue Y, Shinohara Y, Ogawa Y, Sakurai T, Hori H, Kasahara T, et al. Macromolecules 2007;40:2036–45.
[28] Song Y, Nitta K, Nemoto N. Macromolecules 2003;36:1955–61.
[29] Song Y, Nitta K, Nemoto N. Macromolecules 2003;36:8066–73.
[30] Koike Y, Cakmak M. Polymer 2003;44:4249–60.
[31] Li JX, Cheung WL, Chan CM. Polymer 1999;40:2089–102.
[32] Aboulfaraj M, G'Sell C, Ulrich B, Dahoun A. Polymer 1995;36:731–42.
[33] Chu F, Yamaoka T, Kimura Y. Polymer 1995;36:2523–30.
[34] Huy TA, Adhikari R, Lupke T, Henning S, Michler GH. J Polym Sci Part B Polym Phys 2004;42:4478–88.
[35] Galeski A. Prog Polym Sci 2003;28:1643–99.
[36] Darras O, Seguela R. J Polym Sci Part B Polym Phys 1993;31:759–66.
[37] Okane WJ, Young RJ, Ryan AJ. J Macromol Sci Phys 1995;B34:427–58.
[38] Crist B, Fisher CJ, Howard PR. Macromolecules 1989;22:1709–18.
[39] G'Sell C, Jonas J. J Mater Sci 1979;14:583–91.
[40] Duffo P, Monasse B, Haudin JM, G'Sell C, Dahoun A. J Mater Sci 1995;30:701–11.
[41] G'Sell C, Hiver JM, Dahoun A, Souahi A. J Mater Sci 1992;27:5031–9.
[42] Meijer HEH, Govaert LE. Prog Polym Sci 2005;30:915–38.
[43] Jansen BJP, Rastogi S, Meijer HEH, Lemstra PJ. Macromolecules 2001;34:3998–4006.
[44] Jansen BJP, Rastogi S, Meijer HEH, Lemstra PJ. Macromolecules 2001;34:4007–18.
[45] Jansen BJP, Rastogi S, Meijer HEH, Lemstra PJ. Macromolecules 1999;32:6283–9.
[46] van Melick HGH, Govaert LE, Meijer HEH. Polymer 2003;44:3579–91.
[47] Schrauwen BAG, Janssen RPM, Govaert LE, Meijer HEH. Macromolecules 2004;37:6069–78.

[48] Schrauwen BAG, Van Breemen LCA, Spoelstra AB, Govaert LE, Peters GWM, Meijer HEH. Macromolecules 2004;37:8618–33.
[49] Men Y, Rieger J, Strobl G. Phys Rev Lett 2003;91:095502/1–4.
[50] Hiss R, Hobeika S, Lynn C, Strobl G. Macromolecules 1999;32:4390–403.
[51] Hobeika S, Men Y, Strobl G. Macromolecules 2000;33:1827–33.
[52] Picken SJ, Aerts J, Visser R, Northolt MG. Macromolecules 1990;23:3849–54.
[53] Strobl GR, Schnerder M. J Polym Sci Polym Phys Ed 1980;18:1343–59.
[54] Young PJ. Philos Mag 1974;30:85–94.
[55] Shadrake LG, Guiu F. Philos Mag 1976;34:565–81.
[56] Brooks NW, Ghazali M, Duckett RA, Unwin IM, Ward IM. Polymer 1999;40:821–5.
[57] Wunderlich B. Macromolecular physics. In: Crystal nucleation, growth, annealing, vol. 2. New York, London: Academic Press; 1973. p. 13.